

# A variational framework for distortion correction, segmentation and cortical parcellation of diffusion MRI

Oscar Esteban\*, *Member, IEEE*, Alessandro Daducci, *Member, IEEE*, Meritxell Bach-Cuadra, *Member, IEEE*, Jean-Philippe Thiran, *Member, IEEE*, Andrés Santos, *Member, IEEE*, and Dominique Zosso, *Life Fellow, IEEE*

**Abstract**—In whole-brain connectivity analysis of diffusion MRI (dMRI) data, an accurate delineation of the white-matter and grey-matter interfaces is required. While high-standard segmentation is readily available for structural MRI, dMRI typically present significant cerebrospinal fluid contamination effects, mainly derived from its typical low resolution, and severe geometrical distortions. We propose a segmentation-registration variational framework that exploits the detailed anatomy extracted from structural MRI as shape-prior. We use an “active contours without edges”-like model to search for a deformation field that optimally maps the shape prior on multivariate dMRI-derived data in diffusion space, registering structural and diffusion coordinate spaces and implicitly segmenting dMRI data. The approach proven the intrinsic coupling of segmentation and distortion correction and we evaluate its results on a digital simulated phantom and real datasets. Therefore, precise and consistent cortical parcellation on dMRI is straightforward by projection from T1 space, avoiding additional registration, segmentation and/or surface matching steps.

**Index Terms**—diffusion MRI, susceptibility distortion, segmentation, registration, parcellation, shape-prior.

## I. INTRODUCTION

**D**IFFUSION MRI (dMRI) is a widely used family of magnetic resonance (MR) techniques [1] which recently has accounted for a growing interest in its application to whole-brain structural connectivity analysis. This emerging

field [2, 3], currently includes a large amount of imaging techniques for acquisition, processing, and analysis specifically tuned for diffusion MRI (dMRI) data [4].

The whole-brain connectivity analysis has given rise to some challenges towards reliable structural information about the neuronal tracts from dMRI [5, 6]. Here, we shall address brain tissue segmentation on diffusion space and correction of geometrical distortions inherent to the acquisition sequence [7].

In this work, we will refer as brain tissue segmentation to the precise delineation of the cerebrospinal fluid (CSF)-grey matter (GM) and GM-white matter (WM) interface surfaces. An accurate brain tissue segmentation is required to filter the fiber bundles obtained with dMRI tractography. This requirement is usually solved in practice by plainly thresholding the fractional anisotropy (FA), a well-known scalar map derived from dMRI which depicts the isotropy of water diffusion inside the brain. Also, it is necessary to locate the intersections of fiber bundles and GM. Moreover, a precise location of the GM-WM surface is also essential to finally achieve a consistent parcellisation of the cortex to represent the nodes of the output network. This parcellisation is generally defined in a high-resolution and better understood structural magnetic resonance imaging (MRI) of the same subject (e.g. T1-weighted (T1) and/or T2-weighted (T2) weighted acquisitions). Even though some efforts have addressed the study of the robustness of tractography with respect to intra-subject variability [8, 9], these results are restricted to certain regions of the brain, only. Therefore, robust and precise segmentation methods are required in the whole-brain application. The problem is challenging due to the much lower resolution of dMRI (typically around  $2.0 \times 2.0 \times 2.0 \text{ mm}^3$ ) compared to structural MRI, and the existence of geometrical distortions.

dMRI data are usually acquired with echo-planar imaging (EPI) sequences as they allow for very fast acquisitions, but they are known to suffer from geometrical distortions due to local field inhomogeneities. These artifacts happen along the phase-encoding direction, and are most appreciable in the front part of the brain for the strong air/tissue interface around the frontal sinuses. A number of methodologies have been developed to correct for the distortion, and are generically named as *EPI-unwarp* techniques [10, 11, 12, 13]. These methods usually require the extra acquisition of the magnitude and phase of the field (“field-mapping”), a condition which is not always met. Some other methodologies do not make use

Manuscript received XXX XX, 2013; revised XXX XX, 2013. This study is supported by: the Spain’s Ministry of Science and Innovation (projects TEC2010-21619-C04-03, TEC2011-28972-C02-02, CDTI-CENIT AMIT and INNPACTO PRECISION), Comunidad de Madrid (ARTEMIS) and European Regional Development Funds; the Center for Biomedical Imaging (CIBM) of the Geneva and Lausanne Universities and the EPFL, as well as the Leenaards and Louis Jeantet foundations. *Asterisk indicates corresponding author.*

\*O. Esteban is with the Biomedical Image Technologies (BIT), ETSI Telecomunicación, Universidad Politécnica de Madrid and CIBER-BBN, Madrid, Spain, and the Signal Processing Laboratory (LTS5), École Polytechnique Fédérale de Lausanne (EPFL), Lausanne, Switzerland (e-mail: phd@oscaresteban.es).

A. Daducci is with the Signal Processing Laboratory (LTS5), École Polytechnique Fédérale de Lausanne (EPFL), Lausanne, Switzerland.

M. Bach-Cuadra and JP. Thiran are with the Signal Processing Laboratory (LTS5), École Polytechnique Fédérale de Lausanne (EPFL), Lausanne, Switzerland, and Dept. of Radiology, University Hospital Center (CHUV) and University of Lausanne (UNIL), Lausanne, Switzerland.

A. Santos is with the Biomedical Image Technologies (BIT), ETSI Telecomunicación, Universidad Politécnica de Madrid and CIBER-BBN, Madrid, Spain.

D. Zosso is with the Department of Mathematics, University of California, Los Angeles (UCLA), Los Angeles, CA, US and is supported by the Swiss National Science Foundation (SNF) under grant PBELP2-137727.

of the field-mapping, compensating the distortion with non-linear registration from structural MRI or other means [14]. To our knowledge, there exists no study on the impact of the EPI distortion on the variability of tractography results.

Therefore, the problems of precise segmentation in dMRI-space and the spatial mapping between these contours and the corresponding surfaces in anatomical images bear significant redundancy. Once the spatial relationship between T1 and dMRI space is established, the contours which are readily available in T1 space can simply be projected on to the dMRI-data. Conversely, if a precise delineation in dMRI-space was achieved, the spatial mapping with T1-space could be derived from one-to-one correspondences on the contours. However, neither segmentation nor registration can be performed flawlessly, if considered independently. The significant benefits of exploiting the anatomical MRI when segmenting the dMRI data have been demonstrated [15], justifying the use of the shape prior information.

We suggest clustering the current methodologies of template-based segmentation methods into three groups. The first group typically adds a shape prior term to the energy functional of an evolving active contour [16, 17, 18, 19, 20, 21, 22, 23]. These methods generally have a explicit description of the expected relative boundary locations of the object to be delineated, and some even model the statistical deviations from this average shape. Closely related to this group are atlas-based segmentation methods [24, 25, 26, 27, 28], where the prior imposes consistent voxel-based classification of contiguous regions. Here, the presence of more structures than one unique region of interest (ROI) helps aligning the target image with the atlas in a hierarchical fashion. Finally, the third group generalizes the atlas to actual images, and the contour is to segment simultaneously two different target images, related by a spatial transform to be co-estimated [29, 23].

In this paper we propose a novel registration framework to simultaneously solving the segmentation and distortion challenges, by exploiting as strong shape-prior the detailed morphology extracted from high-resolution anatomical MRI. Indeed, hereafter we assume this segmentation problem in anatomical images as a solved by widely used available procedures. Moreover, the shape prior is of very “strong” nature, since it is specific to the particular subject. Also, after global alignment using existing approaches, the remaining spatial deformation between anatomical and diffusion space is due to EPI distortions. Finally, we need to establish precise spatial correspondence between the surfaces in both spaces, including the tangential direction for parcellation. Therefore, we can reduce the problem to finding the differences of spatial distortion in between anatomical and diffusion weighted (DW) space. We thus reformulate the segmentation problem as an inverse problem, where we seek for an underlying deformation field (the distortion) mapping from the structural space into the diffusion space, such that the structural contours segment optimally the dMRI data. In the process, the one-to-one correspondence between the contours in both spaces is guaranteed, and projection of parcellisation to DW space is implicit and consistent.

We test our proposed joint segmentation-registration model

on two different synthetic examples. The first example is a scalar sulcus model, where the CSF-GM boundary particularly suffers from partial volume effect (PVE) and can only be segmented correctly thanks to the shape prior and its coupling with the inner, GM-WM boundary through the imposed deformation field regularity. The second case deals with more realistic dMRI data stemming from phantom simulations of a simplistic brain data. Again, we show that the proposed model successfully segments the dMRI data based on two derived scalar features, namely FA and mean diffusivity (MD), while establishing an estimate of the dense distortion field.

The rest of this paper is organized as follows. First, in section II we introduce our proposed model for joint multivariate segmentation-registration. Then we provide a more detailed description of the data and experimental setup in section III. We present results in section IV and conclude in section V.

## II. METHODS

### A. Mumford-Shah Functional derivation from the Maximum A-Posteriori Model

A widely used approach to image segmentation is derived from the Bayes’ rule (1), where one seeks for a partitioning of a certain image  $X$  in piecewise smooth regions  $\Omega = \{\Omega_k, k \in [1..K]\}$ , that maximizes the a posteriori probability given the multivariate image  $X \in \mathbb{R}^C$ , with  $C$  being the number of image channels.

$$p(Y | X) = \frac{p(X | Y) p(Y)}{p(X)}. \quad (1)$$

Therefore,  $Y$  is a certain realization of the piecewise disjoint region set  $\Omega$ .  $p(X | Y)$  is the *likelihood* of the realization of  $X$  (the image) given a certain distribution model for each region  $\Omega_k$ . The second term,  $p(Y)$ , is the a-priori probability of the partitioning  $Y$ . Finally,  $p(X)$  is the probability of a certain image realization, and thus, it will remain constant when computing the maximum a posteriori (MAP). Consequently,  $p(Y | X) \propto p(X | Y) p(Y)$ , and:

$$\operatorname{argmax}_Y \{p(Y | X)\} = \operatorname{argmax}_Y \{p(X | Y) p(Y)\}. \quad (2)$$

An extended assumption is that the feature vector realization  $X$  is *i.i.d.*, and thus, it is possible to write the a-posteriori probability  $p(X | Y)$  as a continuous product with  $d\mathbf{x}$  the infinitesimal voxel size:

$$p(X | Y) p(Y) = \prod_k \prod_{\mathbf{x} \in \Omega_k} p_k(X(\mathbf{x}) | Y(\mathbf{x}))^{d\mathbf{x}}, \quad (3)$$

where the prior probability  $p(Y)$  is implicitly defined by the regions definition.

A second widely-accepted assumption is the multivariate normal distribution of the different tissues in MRI data. Therefore, the posterior probability of an infinitesimal voxel can be written as:

$$p_k(X(\mathbf{x}) | Y(\mathbf{x})) = \frac{1}{\sqrt{(2\pi)^C |\Sigma_k|}} e^{(-\frac{1}{2} \Delta_k^2(\mathbf{x}(\mathbf{x})))}. \quad (4)$$

where we can identify the factor in the exponential, with  $\mathbf{f} = X(\mathbf{x})$  as the squared *Mahalanobis distance* with the parameters set  $\Theta_k = \{\mu_k, \Sigma_k\}$ :

$$\Delta_k^2(\mathbf{f} | \Theta_k) = (\mathbf{f} - \mu_k)^T \Sigma_k^{-1} (\mathbf{f} - \mu_k). \quad (5)$$

Finally, we can turn the MAP problem into a variational one applying the following log-transform:

$$\begin{aligned} E(X | Y) &= -\log [p(X | Y) p(Y)] = \\ &= -\log \left[ \prod_k \prod_{\mathbf{x} \in \Omega_k} p_k(X(\mathbf{x}) | Y(\mathbf{x})) \right] d\mathbf{x} = \\ &= \sum_k \int_{\Omega_k} -\log [p_k(X(\mathbf{x}) | Y(\mathbf{x}))] d\mathbf{x}, \quad (6) \end{aligned}$$

and introducing the posterior probability term (4), we can express the functional in terms of  $\{\Theta_k, \Omega_k\}$ :

$$\begin{aligned} E(\Theta_k, \Omega_k) &= \\ &= \sum_k \int_{\Omega_k} -\log \left[ \frac{1}{\sqrt{(2\pi)^C |\Sigma_k|}} e^{(-\frac{1}{2} \Delta_k^2(\mathbf{f}))} \right] d\mathbf{x} = \\ &= \sum_k \int_{\Omega_k} \left[ \frac{1}{2} \log((2\pi)^C |\Sigma_k|) + \frac{1}{2} \Delta_k^2(\mathbf{f}) \right] d\mathbf{x}. \quad (7) \end{aligned}$$

Finally, after removing scaling factors and independent constants, we obtain:

$$E(\Theta_k, \Omega_k) = \sum_k \int_{\Omega_k} [\log |\Sigma_k| + \Delta_k^2(\mathbf{f})] d\mathbf{x}, \quad (8)$$

(**FIXME:** bad explanation) where we have a constant term scaled by the total volume of the partition  $\Omega_k$  and the determinant of the covariance matrix of the partition  $|\Sigma_k|$ , plus an energy term based on the squared *Mahalanobis distance*.

Equation (8) resembles the Mumford-Shah functional including variance, that modifies the original functional in a way that it can deal with more general distributions. This is necessary to avoid the assumption that regions  $\Omega_k$  have a fixed covariance matrix on their complete domain. One immediate advantage of this functional from the original one is the possibility to distinguish regions with the same mean vector but different covariance matrix [30]:

$$\begin{aligned} E(\Theta_k, \Omega_k) &= \sum_k \int_{\Omega_k} [\log |\Sigma_k| + \Delta_k^2(\mathbf{f})] d\mathbf{x} \\ &+ \lambda \int_{\Omega_k - K} (|\nabla \mu|^2 + |\nabla \Sigma_k|^2) d\mathbf{x} + \nu |K|, \quad (9) \end{aligned}$$

that is easily identifiable with (8) when we apply the so-called *cartoon limit*, for  $\lambda \rightarrow \infty$ :

$$E(\Theta_k, K) = \sum_k \int_{\Omega_k} [\log |\Sigma_k| + \Delta_k^2(\mathbf{f})] d\mathbf{x} + \nu |K|. \quad (10)$$

As long as we do not penalize the edge set  $K$  length,  $\nu = 0$  and the result is dual to (8):

$$E(\Theta_k, K) = \sum_k \int_{\Omega_k} [\log |\Sigma_k| + \Delta_k^2(\mathbf{f})] d\mathbf{x}. \quad (11)$$

## B. Deformation model

The segmentation problem is transformed into a registration one if the initial partition  $Y$  is derived from the initial shape-priors in reference space. Introducing a dense deformation field  $u$  that maps the original partition to a better fit of the regions in the target coordinate space. Thus, the minimization problem stated in (8) can be expressed so that  $u$  is the unknown:

$$E(u(\mathbf{x})) = \sum_k \int_{\Omega'_k} [\log |\Sigma_k| + \Delta_k^2(\mathbf{f}')] d\mathbf{x} \quad (12)$$

where  $\Omega'_k = u(\Omega_k)$  and  $\mathbf{f}' = X(u(\mathbf{x}))$ .

## C. Active contours without edges based segmentation model

Let us denote  $\{c_i\}_{i=1..N_e}$  the nodes of a shape prior surface. In our application, a precise WM-GM interface extracted from a high-resolution reference volume. All the formulations can be naturally extended to include more shape priors. On the other hand, we have a number of dMRI-derived features at each voxel of the volume. Let us denote by  $x$  the voxel and  $f(x) = [f_1, f_2, \dots, f_N]^T(x)$  its associated feature vector.

The transformation from reference into dMRI coordinate space is achieved through a dense deformation field  $u(x)$ , such that:

$$c'_i = T\{c_i\} = c_i + u(c_i) \quad (13)$$

Since the nodes of the anatomical surfaces might lay off-grid, it is required to derive  $u(x)$  from a discrete set of parameters  $\{u_k\}_{k=1..K}$ . Densification is achieved through a set of associated basis functions  $\Psi_k$  (e.g. rbf, interpolation splines):

$$u(x) = \sum_k \Psi_k(x) u_k \quad (14)$$

Consequently, the transformation writes

$$c'_i = T\{c_i\} = c_i + u(c_i) = c_i + \sum_k \Psi_k(c_i) u_k \quad (15)$$

Based on the current estimate of the distortion  $u$ , we can compute “expected samples” within the shape prior projected into the dMRI. Thus, we now estimate region descriptors of the dMRI features  $f(x)$  of the regions defined by the priors in dMRI space. Using Gaussian distributions as region descriptors, we propose an active contours without edges (ACWE)-like, piece-wise constant, variational image segmentation model (where the unknown is the deformation field) [31]:

where  $R$  indexes the existing regions and the integral domains depend on the deformation field  $u$ . Note that minimizing this energy,  $\argmin_u \{E\}$ , yields the MAP estimate of a piece-wise smooth image model affected by Gaussian additive noise. This inverse problem is ill-posed [32, 33]. In order to account for deformation field regularity and to render the problem well-posed, we include limiting and regularization terms into the energy functional [34, 35]:

$$\begin{aligned} E(u) &= \sum_{\forall R} \left\{ \int_{\Omega_R} (f - \mu_R)^T \Sigma_R^{-1} (f - \mu_R) dx \right\} \\ &+ \alpha \int \|u\|^2 dx + \beta \int (\|\nabla u_x\|^2 + \|\nabla u_y\|^2 + \|\nabla u_z\|^2) dx \quad (16) \end{aligned}$$

These regularity terms ensure that the segmenting contours in dMRI space are still close to their native shape. The model easily allows to incorporate inhomogeneous and anisotropic regularization [36] to better regularize the EPI distortion.

At each iteration, we update the distortion along the steepest energy descent. This gradient descent step can be efficiently tackled by discretizing the time in a forward Euler scheme, and making the right hand side semi-implicit in the regularization terms:

$$\frac{u^{t+1} - u^t}{\tau} = - \sum_{i=1}^{N_c} [e(f(c'_i)) \hat{n}_{c'_i} \Psi_{c_i}(x)] - \alpha u^{t+1} + \beta \Delta u^{t+1} \quad (17)$$

where the data terms remain functions of the current estimate  $u^t$ , thus  $c'_i = c'_i(u^t)$ . For simplicity on notation, we restricted the number of priors to only 1. We also defined  $e(f(c'_i)) = E_{out}(f(c'_i)) - E_{in}(f(c'_i))$ , and  $E_R(f) = (f - \mu_R)^T \Sigma_R^{-1} (f - \mu_R)$ . We applied a spectral approach to solve this implicit scheme:

$$u^{t+1} = \mathcal{F}^{-1} \left\{ \frac{\mathcal{F}\{u^t/\tau - \sum_{i=1}^{N_c} [e(f(c'_i)) \hat{n}_{c'_i} \Psi_{c_i}(x)]\}}{\mathcal{F}\{(1/\tau + \alpha)\mathcal{I} - \beta\Delta\}} \right\} \quad (18)$$

### III. DATA AND EXPERIMENTS

#### A. Image Data

1) *Simulated digital phantom*: The lack of a widely accepted *gold-standard* in the application field has been addressed by several authors [37]. In this work, we use one of the most complete, and publicly available, digital phantoms ([http://hardi.epfl.ch/static/events/2013\\_ISBI/testing\\_data.html](http://hardi.epfl.ch/static/events/2013_ISBI/testing_data.html)). The phantom is a spherical volume containing a set of fiber bundles, that connect one area of a “cortex” to another. The model accounts for PVE using a similar approach to [38] and for CSF contamination as well.

2) *Real MRI datasets*: We used image data from XX healthy volunteers with no history of neurological conditions (ages XX±XX, X female) to illustrate the applicability of our approach. All the subjects were scanned in a 3T MR Scanner (Siemens Magnetom TrioTim, Siemens, Erlangen, Germany) with a standard 12-channel head coil. (**FIXME**: check coil number of channels!!) Subjects were scanned twice with the same protocol, described hereafter. After being scanned the first time, each subject exited the scan room for a short break and then reentered for an identical scan session. To note, there was a full repositioning of the volunteer, coils, blankets and pads before each scan and re-scan session. The scan session protocol was as follows:

- 1) Triplanar survey (Localizer).
- 2) Field Mapping: field mapping using GRE sequence was performed before dMRI acquisition for susceptibility correction purposes.
- 3) DTI: dMRI were acquired with axial in-plane isotropic resolution 2mm, slice thickness 2mm, XXXX×XXX×XXX image matrix, TR= XXXX ms, TE = XX ms,

NEX = X, BW = XXXX Hz/pixel, GRAPPA acceleration factor 2. The series included images acquired with diffusion weighting along 30 non-collinear directions ( $b=700\text{sm}^{-2}$ ) sampled twice for averaging, and 5 interleaved images acquired without diffusion weighting ( $b=0$ ).

- 4) Field Mapping (same as before DTI)
- 5) Structural T1: An MPRAGE T1-weighted acquisition, sagittal GRE sequence, in-plane isotropic resolution 1.0 mm, slice thickness 1.2mm XXX×XXX×XXX image matrix, TR=2300 ms, TE=2.98 ms, FA= 9, NEX=X, BW= 240 Hz/pixel.
- 6) Structural T2: A T2-weighted acquisition, oblique axial TSE sequence, in-plane isotropic resolution 1.0 mm, slice thickness 1.2mm XXX×XXX×XXX image matrix, TR=3200 ms, TE= 408 ms, NEX=X, BW= 751 Hz/pixel.

#### B. Image preprocessing and shape-prior generation

Regardless the dataset type (simulated or real), all dMRI datasets were processed using the standard diffusion tensor imaging (DTI) reconstruction methods provided by FSL<sup>1</sup> to fit the tensor model and produce scalar maps of the required features. The properties of the reconstructed tensors and derived scalar maps have been studied by [39]. Based on their findings, FA (19) and MD (20) are considered complementary features, and therefore we selected them for the energy model (16) in driving the registration-segmentation process. Whereas FA informs mainly about the *shape* of diffusion, the MD is more related to the *magnitude* of the process:

$$\text{FA} = \sqrt{\frac{1}{2} \frac{\sqrt{(\lambda_1 - \lambda_2)^2 + (\lambda_2 - \lambda_3)^2 + (\lambda_3 - \lambda_1)^2}}{\sqrt{\lambda_1^2 + \lambda_2^2 + \lambda_3^2}}} \quad (19)$$

$$\text{MD} = (\lambda_1 + \lambda_2 + \lambda_3)/3 \quad (20)$$

where  $\lambda_i$  are the eigenvalues of the diffusion tensor associated with the diffusion signal  $S(\vec{q})$ . There exist two main reasons to justify their choice. First, they are well-understood and standardized in clinical routine. Second, together they contain most of the information that is usually extracted from the dMRI-derived scalar maps [39].

Preprocessing differed between simulated and real datasets in the shape-prior surfaces generation, as we describe hereafter.

1) *Simulated digital phantom*: A description goes here: surfaces extraction, synthetic susceptibility artifact generation.

2) *Real MRI data*: We used a standard automated method available in *FreeSurfer* [40] to obtain the cortical gray/white boundary from the T1 scan [41]. Parcellations used to evaluate the repeatability of the method are also obtained from *FreeSurfer*.

#### C. Experiments and evaluation

<sup>1</sup>DTIFIT, included in the FMRIB's Software Library (FSL), [http://fsl.fmrib.ox.ac.uk/fsl/fsl-4.1.9/fdt/fdt\\_dtifit.html](http://fsl.fmrib.ox.ac.uk/fsl/fsl-4.1.9/fdt/fdt_dtifit.html)

1) *Validation on the simulated digital phantom:* We firstly evaluated our approach on the simulated data, using the distorted data with a deformation field similar to the susceptibility artifact that affects real dMRI data. To this end, we report the following indices:

- Surface error (SE), a distance between the one-to-one corresponding vertices, weighted by their respective Voronoi area.

$$MSE = \sum_k \sum_j^M w_j \|\mathbf{x}_j - \hat{\mathbf{x}}_j\| \quad (21)$$

where  $\mathbf{x}_j$  are the locations of the  $M$  vertices of the  $k$  priors,  $\hat{\mathbf{x}}_j$  are the corresponding locations recovered, and  $w_j$  the weighting factor as the relative surface of the Voronoi area.

- Warping index (WI), L2-distance between the theoretical and the recovered deformation field.

$$WI = \frac{1}{N} \sum_i^N \|\mathbf{d}_i - \hat{\mathbf{d}}_i\| \quad (22)$$

where  $\mathbf{d}_i$  is the theoretical displacement vector at position  $i$  and  $\hat{\mathbf{d}}_i$  is the recovered one at the same index position.

- Parcellation agreement, the SE averaged by defined ROIs between the theoretical and the recovered parcellations.
- number of fibers (NoF) agreement, between the fibers recovered on the original data and the processed data.

Additionally, the entropy of data is studied in both original and recovered datasets to draw another possible basis for the assessment of the real datasets. We also report the same indices for the outcome of a widely-used methodology that combines field-map susceptibility correction and T1-T2-dMRI registration (**FIXME**: I suggest to give it a compact name and define it in the pre-processing section or even before in the intro).

2) *Evaluation on real datasets:* For the real datasets there is no published *gold-standard* to validate results. Thus, visual results are provided to let compare the performance with the NICEACRONYM standard methodology. Additionally, cross-comparison of repeatability results are provided. In this second evaluation strategy, all the indices defined in subsubsection III-C1 are reported.

#### IV. RESULTS AND DISCUSSION

Please! Write me ASAP.

#### V. CONCLUSION

A novel application for the ACWE framework is proposed, with the aim at recovering the displacement field underlying the EPI geometrical distortions. Exploiting the segmentation properties of the ACWE and optimizing the displacement field, we describe a registration-segmentation methodology that simultaneously segmented and restored the distortion on dMRI-like synthetic data. Visual results and quantitative results are provided.

We implemented the methodology upon the widely used Insight Registration and Segmentation Toolkit <sup>2</sup> (ITK) for its

computational benefits, the standardized code, and with the aim at making the procedure publicly available when ready for sharing with the research community.

Once proven the aptness of the methodology to the application with simplistic synthetic data, in further studies we will cover the actual performance on real images and the benefits of overcoming the described challenges (segmentation and EPI distortion correction) in one single step. Additional research lines regard with the use of more adequate optimization schemes and the use of an energy model better adapted to the specific nature of the dMRI data.

We conclude recalling the importance of tackling with the numerous challenges that exist on the dMRI data processing in order to achieve reliable results on the whole-brain connectivity analysis.

#### ACKNOWLEDGMENT

The authors gratefully acknowledge V. Estellers for critical discussions at early stages of this project, A. Griffa for acquiring the real datasets used in this work, K. O'Brien for his discussions and clarifications regarding distortions and their foundations in dMRI, E. Caruyer for providing us with the simulated digital phantom, and L. Vese for her generous support.

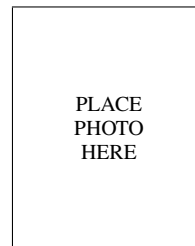
#### REFERENCES

- [1] P. C. Sundgren, Q. Dong, D. Gómez-Hassan, S. K. Mukherji, P. Maly, and R. Welsh, "Diffusion tensor imaging of the brain: review of clinical applications," *Neuroradiology*, vol. 46, pp. 339–350, May 2004. [Online]. Available: <http://www.springerlink.com/content/fa30k4q3h9kg4yjq/>
- [2] P. Hagmann, "From diffusion MRI to brain connectomics," Ph.D. dissertation, Institut de traitement des signaux PROGRAMME DOCTORAL EN INFORMATIQUE ET COMMUNICATIONS POUR L'OBTENTION DU GRADE DE DOCTEUR ÈS SCIENCES PAR Docteur en médecine, Université de Lausanne, 2005. [Online]. Available: [http://biblion.epfl.ch/EPFL/theses/2005/3230/EPFL\\_TH3230.pdf](http://biblion.epfl.ch/EPFL/theses/2005/3230/EPFL_TH3230.pdf)
- [3] O. Sporns, G. Tononi, and R. Kötter, "The human connectome: A structural description of the human brain," *PLoS computational biology*, vol. 1, no. 4, p. e42, Sep. 2005, PMID: 16201007.
- [4] A. Daducci, S. Gerhard, A. Griffa, A. Lemkaddem, L. Cammoun, X. Gigandet, R. Meuli, P. Hagmann, and J.-P. Thiran, "The connectome mapper: An open-source processing pipeline to map connectomes with MRI," *PLoS ONE*, vol. 7, no. 12, p. e48121, Dec. 2012. [Online]. Available: <http://dx.doi.org/10.1371/journal.pone.0048121>
- [5] H. Johansen-Berg and M. F. Rushworth, "Using diffusion imaging to study human connective anatomy," *Annual Review of Neuroscience*, vol. 32, no. 1, pp. 75–94, 2009, PMID: 19400718. [Online]. Available: <http://www.annualreviews.org/doi/abs/10.1146/annurev.neuro.051508.135735>

<sup>2</sup><http://www.itk.org>

- [6] D. K. Jones, T. R. Knösche, and R. Turner, "White matter integrity, fiber count, and other fallacies: The do's and don'ts of diffusion MRI," *NeuroImage*, Jul. 2012, PMID: 22846632.
- [7] P. Hagmann, P. E. Grant, and D. A. Fair, "MR connectomics: a conceptual framework for studying the developing brain," *Frontiers in Systems Neuroscience*, vol. 6, Jun. 2012, PMID: 22707934 PMCID: PMC3374479. [Online]. Available: <http://www.ncbi.nlm.nih.gov/pmc/articles/PMC3374479/>
- [8] E. Heiervang, T. Behrens, C. Mackay, M. Robson, and H. Johansen-Berg, "Between session reproducibility and between subject variability of diffusion MR and tractography measures," *NeuroImage*, vol. 33, no. 3, pp. 867–877, Nov. 2006. [Online]. Available: <http://www.sciencedirect.com/science/article/pii/S1053811906008081>
- [9] S. Wakana, A. Caprihan, M. M. Panzenboeck, J. H. Fallon, M. Perry, R. L. Gollub, K. Hua, J. Zhang, H. Jiang, P. Dubey, A. Bliz, P. van Zijl, and S. Mori, "Reproducibility of quantitative tractography methods applied to cerebral white matter," *NeuroImage*, vol. 36, no. 3, pp. 630–644, Jul. 2007. [Online]. Available: <http://www.sciencedirect.com/science/article/pii/S1053811907001383>
- [10] D. Holland, J. M. Kuperman, and A. M. Dale, "Efficient correction of inhomogeneous static magnetic field-induced distortion in echo planar imaging," *NeuroImage*, vol. 50, no. 1, p. 175, Mar. 2010, PMID: 19944768 PMCID: PMC2819607. [Online]. Available: <http://www.ncbi.nlm.nih.gov/pmc/articles/PMC2819607/>
- [11] Y.-C. Hsu, C.-H. Hsu, and W.-Y. Tseng, "Correction for susceptibility-induced distortion in echo-planar imaging using field maps and model-based point spread function," *IEEE Transactions on Medical Imaging*, vol. 28, no. 11, pp. 1850–1857, Nov. 2009.
- [12] P. Jezard, A. S. Barnett, and C. Pierpaoli, "Characterization of and correction for eddy current artifacts in echo planar diffusion imaging," *Magnetic resonance in medicine*, vol. 39, no. 5, p. 801–812, 2005. [Online]. Available: <http://onlinelibrary.wiley.com/doi/10.1002/mrm.1910390518/abstract>
- [13] P. J. Reber, E. C. Wong, R. B. Buxton, and L. R. Frank, "Correction of off resonance-related distortion in echo-planar imaging using EPI-based field maps," *Magnetic Resonance in Medicine*, vol. 39, no. 2, p. 328–330, 2005. [Online]. Available: <http://onlinelibrary.wiley.com/doi/10.1002/mrm.1910390223/abstract>
- [14] J. L. R. Andersson, C. Hutton, J. Ashburner, R. Turner, and K. Friston, "Modeling geometric deformations in EPI time series," *Neuroimage*, vol. 13, no. 5, p. 903–919, 2001. [Online]. Available: <http://www.sciencedirect.com/science/article/pii/S1053811901907463>
- [15] L. Zöllei, A. Stevens, K. Huber, S. Kakunoori, and B. Fischl, "Improved tractography alignment using combined volumetric and surface registration," *NeuroImage*, vol. 51, no. 1, pp. 206–213, May 2010. [Online]. Available: <http://www.sciencedirect.com/science/article/pii/S1053811910001400>
- [16] X. Bresson, P. Vandergheynst, and J. P. Thiran, "A variational model for object segmentation using boundary information and shape prior driven by the mumford-shah functional," *International Journal of Computer Vision*, vol. 68, no. 2, p. 145–162, 2006. [Online]. Available: <http://www.springerlink.com/index/WU0311444417743P.pdf>
- [17] T. Chan and W. Zhu, "Level set based shape prior segmentation," in *Computer Vision and Pattern Recognition, 2005. CVPR 2005. IEEE Computer Society Conference on*, vol. 2, 2005, p. 1164–1170. [Online]. Available: [http://ieeexplore.ieee.org/xpls/abs\\_all.jsp?arnumber=1467575](http://ieeexplore.ieee.org/xpls/abs_all.jsp?arnumber=1467575)
- [18] Y. Chen, H. D. Tagare, S. Thiruvankadam, F. Huang, D. Wilson, K. S. Gopinath, R. W. Briggs, and E. A. Geiser, "Using prior shapes in geometric active contours in a variational framework," *International Journal of Computer Vision*, vol. 50, no. 3, pp. 315–328, Dec. 2002. [Online]. Available: <http://link.springer.com/article/10.1023/A%3A1020878408985>
- [19] D. Cremers, S. J. Osher, and S. Soatto, "Kernel density estimation and intrinsic alignment for shape priors in level set segmentation," *International Journal of Computer Vision*, vol. 69, no. 3, p. 335–351, May 2006.
- [20] M. Gastaud, M. Barlaud, and G. Aubert, "Combining shape prior and statistical features for active contour segmentation," *IEEE Transactions on Circuits and Systems for Video Technology*, vol. 14, no. 5, p. 726–734, May 2004.
- [21] N. Paragios, "A level set approach for shape-driven segmentation and tracking of the left ventricle," *IEEE Transactions on Medical Imaging*, vol. 22, no. 6, p. 773–776, Jun. 2003.
- [22] B. Vemuri and Y. Chen, "Joint image registration and segmentation," in *Geometric Level Set Methods in Imaging, Vision, and Graphics*. New York: Springer-Verlag, 2003, p. 251–269.
- [23] A. Yezzi, L. Zöllei, and T. Kapur, "A variational framework for integrating segmentation and registration through active contours," *Medical Image Analysis*, vol. 7, no. 2, p. 171–185, Jun. 2003.
- [24] S. Gorthi, V. Duay, N. Houhou, M. Bach Cuadra, U. Schick, M. Becker, A. S. Allal, and J.-P. Thiran, "Segmentation of head and neck lymph node regions for radiotherapy planning using active contour-based atlas registration," *IEEE Journal of Selected Topics in Signal Processing*, vol. 3, no. 1, p. 135–147, 2009.
- [25] S. Gorthi, V. Duay, X. Bresson, M. Bach Cuadra, F. J. Sánchez Castro, C. Pollo, A. S. Allal, and J.-P. Thiran, "Active deformation fields: dense deformation field estimation for atlas-based segmentation using the active contour framework," *Medical Image Analysis*, vol. 15, no. 6, p. 787–800, 2011.
- [26] K. M. Pohl, J. Fisher, J. J. Levitt, M. E. Shenton, R. Kikinis, W. E. L. Grimson, and W. M. Wells, "A unifying approach to registration, segmentation, and intensity correction," in *MICCAI 2005*, ser. Lecture Notes in

- Computer Science, J. S. Duncan and G. Gerig, Eds., vol. 3749. Berlin, Heidelberg: Springer Berlin Heidelberg, 2005, p. 310–318.
- [27] K. M. Pohl, J. Fisher, W. E. L. Grimson, R. Kikinis, and W. M. Wells, “A bayesian model for joint segmentation and registration,” vol. 31, no. 1, p. 228–39, May 2006.
- [28] F. Wang, B. C. Vemuri, and S. J. Eisenschenk, “Joint registration and segmentation of neuroanatomic structures from brain MRI,” *Academic radiology*, vol. 13, no. 9, p. 1104–11, Sep. 2006.
- [29] P. P. Wyatt and J. Noble, “MAP MRF joint segmentation and registration of medical images,” *Medical Image Analysis*, vol. 7, no. 4, p. 539–552, Dec. 2003.
- [30] T. Brox and D. Cremers, “On local region models and a statistical interpretation of the piecewise smooth mumford-shah functional,” *International Journal of Computer Vision*, vol. 84, no. 2, pp. 184–193, Aug. 2009. [Online]. Available: <http://link.springer.com/article/10.1007/s11263-008-0153-5>
- [31] T. F. Chan and L. A. Vese, “Active contours without edges,” *IEEE Transactions on Image Processing*, vol. 10, no. 2, p. 266–277, 2001.
- [32] M. Bertero, T. A. Poggio, and V. Torre, “Ill-posed problems in early vision,” in *Proceedings of the IEEE*, vol. 76, 1988, p. 869–889.
- [33] J. Hadamard, “Sur les problèmes aux dérivées partielles et leur signification physique,” *Princeton University Bulletin*, vol. 13, p. 49–52, 1902.
- [34] V. A. Morozov, “Linear and nonlinear ill-posed problems,” *Journal of Mathematical Sciences*, vol. II, no. 6, p. 706–736, 1975.
- [35] A. N. Tichonov, “Solution of incorrectly formulated problems and the regularization method,” *Soviet Mathematics*, vol. 4, p. 1035–1038, 1963.
- [36] H.-H. Nagel and W. Enkelmann, “An investigation of smoothness constraints for the estimation of displacement vector fields from image sequences,” *IEEE Transactions on Pattern Analysis and Machine Intelligence*, vol. PAMI-8, no. 5, p. 565–593, Sep. 1986. [Online]. Available: <http://ieeexplore.ieee.org/lpdocs/epic03/wrapper.htm?arnumber=4767833>
- [37] M.-A. Côté, G. Girard, A. Boré, E. Garyfallidis, J.-C. Houde, and M. Descoteaux, “Tractometer: Towards validation of tractography pipelines,” *Medical Image Analysis*, 2013. [Online]. Available: <http://www.sciencedirect.com/science/article/pii/S1361841513000479>
- [38] T. G. Close, J.-D. Tournier, F. Calamante, L. A. Johnston, I. Mareels, and A. Connolly, “A software tool to generate simulated white matter structures for the assessment of fibre-tracking algorithms,” *Neuroimage*, vol. 47, no. 4, pp. 1288–1300, Oct. 2009, PMID: 19361565.
- [39] D. B. Ennis and G. Kindlmann, “Orthogonal tensor invariants and the analysis of diffusion tensor magnetic resonance images,” *Magnetic Resonance in Medicine*, vol. 55, no. 1, p. 136–146, 2006. [Online]. Available: <http://onlinelibrary.wiley.com/doi/10.1002/mrm.20741/abstract>
- [40] B. Fischl, “FreeSurfer,” *NeuroImage*, vol. 62, no. 2, pp. 774–781, Aug. 2012. [Online]. Available: <http://www.sciencedirect.com/science/article/pii/S1053811912000389>
- [41] D. N. Greve and B. Fischl, “Accurate and robust brain image alignment using boundary-based registration,” *NeuroImage*, vol. 48, no. 1, pp. 63–72, Oct. 2009, PMID: 19573611.



**Oscar Esteban** Biography text here.